Songklanakarin J. Sci. Technol.
39 (2), 143-151, Mar. - Apr. 2017

http://www.sjst.psu.ac.th

Review Article

Effects of intermediate principal stress on creep closure of storage caverns in Maha Sarakham salt

Sarayuth Archeeploha, Supattra Khamrat, and Kittitep Fuenkajorn*

Geomechanics Research Unit, Institute of Engineering,
Suranaree University of Technology, Mueang, Nakhon Ratchasima, 30000 Thailand

Received: 9 August 2015; Revised: 6 April 2016; Accepted: 5 May 2017

Abstract

True triaxial creep tests are performed to determine the effects of the intermediate principal stress on the time-dependent behavior of the Maha Sarakham salt. The applied octahedral shear stresses vary from 5 to 14 MPa while the mean stress is maintained constant at 15 MPa. The loading conditions include conventional triaxial compression, polyaxial and triaxial extension testing. Regression analyses of the results based on the Burgers model indicate that the instantaneous deformation tends to be independent of σ_2. The visco-elastic and visco-plastic parameters notably increase with σ_2. To calculate the σ_2 effect on the long-term closure of salt storage caverns the Burgers parameters are defined as a function of the Lode parameter. The results indicate that the conventional creep test results may overestimate the actual closure of cylindrical and spherical caverns by as much as 15% and 35%, respectively.

Keywords: rock salt, creep, true triaxial, intermediate principal stress, closure

1. Introduction

The effects of confining pressures on the mechanical properties of rocks are commonly simulated in a laboratory by performing triaxial compression testing of cylindrical rock core specimens. A significant limitation of these conventional methods is that the intermediate and minimum principal stresses are equal during the test while the actual in-situ rock is normally subjected to an orthotropic stress state where the maximum, intermediate and minimum principal stresses are different ($\sigma_1>\sigma_2>\sigma_3>0$). It has been found that compressive strengths obtained from conventional triaxial testing cannot represent the actual in-situ strength where the rock is subjected to an anisotropic stress state (Haimson, 2006; Haimson & Chang, 2000; Hunsche, 1984; Tiwari & Rao, 2004, 2006; Yang, Zou, & Sui 2007).

* Corresponding author.
Email address: kittitep@sut.ac.th

From the experimental results on brittle rocks obtained by Haimson (2006) and Colmenares & Zoback (2002) it can be generally concluded that in a σ_1–σ_2 diagram, for a given σ_3, σ_1 at failure initially increases with σ_2 to a certain magnitude, and then it gradually decreases as s_2 increases. The effect of σ_2 is larger under higher σ_3. Cai (2008) offers an explanation of how the intermediate principal stress affects the rock strength based on the results from numerical simulations on fracture initiation and propagation. He states that the intermediate principal stress confines the rock in such a way that fractures can only be initiated and propagated in the direction parallel to σ_1 and σ_2. The effect of σ_2 is related to the stress-induced anisotropic properties and behavior of the rock and to the end effect at the interface between the rock surface and loading platen in the direction of the σ_2 application. The effect should be smaller in homogeneous and fine-grained rocks than in coarse-grained rocks where pre-existing micro-cracks are not uniformly distributed.

Phueakphum, Fuenkajorn, and Walsri (2013) study the effect of intermediate principal stress on tensile strength

of sandstone. The results indicate that the compressive and tensile strengths and cohesion obtained from the triaxial extension tests ($\sigma_1 = \sigma_2$) are greater than from the triaxial compression tests ($\sigma_2 = \sigma_3$).

Several failure criteria have been developed to describe the rock strength under true triaxial stress states. Comprehensive reviews of these criteria have been given recently by Haimson (2006), Colmenares and Zoback (2002), Cai (2008), Al-Ajmi and Zimmerman (2005), Benz and Schwab (2008), and You (2009). Among several other criteria, the Mogi (You, 2009) and modified Wiebols and Cook (Colmenares & Zoback, 2002; Zhou, 1994) criteria are perhaps the most widely used to describe the rock compressive strengths under true triaxial stresses.

Even through the effect of σ_2 on rock strengths has long been recognized and studied as mentioned above, the σ_2 effect on time-dependent deformation of rocks has rarely been addressed. The experimental investigation on their issue is very limited. Mellegard, DeVries, and Callahan (2007) describe the steady-state creep rate of salt by considering the intermediate principal stress. From limited experiment data it has been concluded that the Lode angle does not affect the steady-state strain rate of salt. The transient strain rate might be slightly higher in triaxial extension than triaxial compression. The knowledge and understanding of the σ_2 effect on salt creep are however important for the determination or prediction of the long-term closure of compressed-air energy and gas storage caverns in salt. Such closure will dictate the efficiency and capacity of the storage operation.

The objective of this study is to experimentally determine the effects of the intermediate principal stress on the instantaneous and time-dependent deformation of rock salt obtained from the Maha Sarakham formation. True triaxial creep testing has been performed on rectangular salt specimens with loading conditions varying from triaxial compression ($\sigma_1>\sigma_2=\sigma_3$), polyaxial ($\sigma_1>\sigma_2>\sigma_3$), to triaxial extension ($\sigma_1=\sigma_2>\sigma_3$). The Burgers model is used to describe the elastic, visco-elastic and visco-plastic deformations of the salt specimen tested under various stress states. Radial closure of spherical and cylindrical gas storage caverns in the Maha Sarakham salt is calculated to compare the results obtained from testing under different loading conditions.

2. Salt Specimens

The tested specimens have been prepared from 60 mm salt cores drilled from the depths ranging between 160 m and 270 m by Pimai Salt Co. in the northeast of Thailand. The salt cores belong to the Middle salt member of the Maha Sarakham formation in the Khorat basin. This salt formation hosts several solution-mined caverns in the basin. It is also being considered as a host rock for compressed-air energy storage caverns by the Thai Department of Energy, and for chemical waste disposal by the Office of Atomic Energy for Peace. Warren (1999) describes the origin and geological structures of the Maha Sarakham salt. The salt cores used here are virtually pure halite with average grain (crystal) sizes of 5×5×5 mm. The salt cores have been dry-cut to obtain rectangular blocks with nominal dimensions of 54×54×108 mm. No bedding is observed in the specimens.

3. Test Method

The tests are categorized into three series based on the loading conditions: triaxial compression ($\sigma_1>\sigma_2=\sigma_3$), polyaxial ($\sigma_1>\sigma_2>\sigma_3$), and triaxial extension ($\sigma_1=\sigma_2>\sigma_3$). The applied constant octahedral shear stresses range from 5, 8, 11 to 14 MPa which are used, as much as practical, for all stress conditions. All specimens are tested under the same mean stress of 15 MPa, primarily to isolate the effect of confinement from the test results. Table 1 shows the magnitudes of the applied principal stresses and their corresponding

Table 1. Loading conditions used for true triaxial creep testing.

Specimen No.	Depth (m)	Loading Conditions	Density (g/cm^3)	Constant Principal Stresses			τ_{oct} (MPa)
				σ_1 (MPa)	σ_2 (MPa)	σ_3 (MPa)	
TC-2	209.68-209.80	$\sigma_1\neq\sigma_2=\sigma_3$	2.18	34.8	5.1	5.1	14.0
TC-11	255.67-256.02		2.18	30.6	7.2	7.2	11.0
TC-13	238.22-238.28		2.15	26.3	9.4	9.4	8.0
TC-16	162.82-162.88		2.17	22.1	11.5	11.5	5.0
TC-20	204.10-204.15	$\sigma_1\neq\sigma_2\neq\sigma_3$	2.14	34.6	7.2	3.2	14.0
TC-19	204.02-204.06		2.14	30.6	8.2	6.2	11.1
TC-14	268.32-268.38		2.17	26.3	10.3	8.3	8.1
TC-17	162.74-162.80		2.21	21.5	14.3	9.3	5.0
TC-4	253.64-253.75	$\sigma_1=\sigma_2\neq\sigma_3$	2.09	21.0	21.0	3.0	8.5
TC-8	208.30-208.40		2.15	20.0	20.0	5.0	7.1
TC-18	202.14-202.26		2.17	18.6	18.6	7.9	5.0

octahedral shear stress for each specimen.

A polyaxial load frame (Fuenkajorn, Sriapai, & Samsri, 2012) has been used to apply constant axial stress (σ_1) and lateral stresses (σ_2 and σ_3) to the salt specimens. After installing into the center of the load frame, the salt specimen is secured by six loading platens arranged in three mutually perpendicular directions. The loading areas of the platens are slightly smaller than the specimen dimensions. The top and bottom platens have the loading area of 52×52 mm^2. The four lateral platens have loading area of 52×106 mm. This allows axial and lateral deformations of the specimens during testing. Neoprene sheets are placed at the interfaces between the platens and specimen surfaces. The pre-calculated dead weights are placed on the two lower beams to obtain the lateral stress of 15 MPa along the two mutually perpendicular directions. Simultaneously the axial (vertical) stress is increased to 15 MPa. This uniform stress is maintained for a minimum of one hour primarily to ensure that the salt specimen is under isostatic condition. The applied stresses are then adjusted to obtain the pre-defined octahedral shear stresses (τ_{oct}) while the mean stresses are maintained at 15 MPa. They are calculated from the three principal stresses as (Jaeger, Cook, & Zimmerman, 2007):

$$\tau_{oct} = 1/3\{(\sigma_1-\sigma_2)^2+(\sigma_2-\sigma_3)^2+(\sigma_3-\sigma_1)^2\}^{1/2} \quad (1)$$

$$\sigma_m = (\sigma_1+\sigma_2+\sigma_3)/3 \quad (2)$$

Each specimen is tested up to 21 days. The deformations along the principal axes are monitored using displacement digital gages. The readings are made every one minute for the first three hours. The reading intervals are gradually increased to every hour after five days of testing. All tests are conducted under ambient temperature (25-28 degree Celsius).

4. Test Results

Figure 1 shows the principal strains (ε_1, ε_2, ε_3) and volumetric strains (ε_v) as a function of time for all tested specimens. The curves show the instantaneous, transient and steady-state creep phases of the salt. For all loading conditions the axial strains increase with τ_{oct}. Under the triaxial compression loading ($\sigma_1>\sigma_2=\sigma_3$) the intermediate and minor principal strain curves are virtually identical. Under the triaxial extension loading ($\sigma_1=\sigma_2>\sigma_3$) the major and intermediate principal strain curves are comparable. These suggest that the test procedure and measurement techniques are sufficiently reliable. The octahedral shear strains (γ_{oct}) are plotted as a function of time in Figure 2, where they are calculated by (Jaeger *et al.*, 2007):

$$\gamma_{oct} = 1/3\{(\varepsilon_1-\varepsilon_2)^2+(\varepsilon_2-\varepsilon_3)^2+(\varepsilon_3-\varepsilon_1)^2\}^{1/2} \quad (3)$$

The results suggest that under the same magnitude of τ_{oct} the specimens under triaxial compression ($\sigma_1>\sigma_2=\sigma_3$) show larger creep strains than those under polyaxial ($\sigma_1>\sigma_2>\sigma_3$) and triaxial extension ($\sigma_1=\sigma_2>\sigma_3$) conditions.

5. Burgers Model

The Burgers model is used to describe the test results primarily because it is simple and capable of describing the elastic, visco-elastic and visco-plastic phases of the salt creep under isothermal condition. It is recognized that numerous creep models or constitutive equations have been developed to represent the time-dependent behavior of rock salt. They are however complex and cannot isolate each phase of salt creep. Figure 3 shows the physical components arranged in the Burgers model. Assuming that the salt is isotropic and linearly elastic a relation between octahedral shear strain and stress can be written as (Jaeger *et al.*, 2007):

$$\gamma_{oct} = \tau_{oct} / 2G \quad (4)$$

where G is the shear modulus of the salt. Using the Laplace transformation a linear visco-elastic relation can be derived from the above equation by using time operator of the Burgers model, and hence the octahedral shear strain can be presented as a function of time (Richards, 1993):

$$\gamma_{oct}(t) = \tau_{oct}[(t/\eta_1) + (1/E_1) + (1/E_2)(1-\exp(E_2\times t/\eta_2))] \quad (5)$$

where τ_{oct} is the applied constant octahedral shear stresses (MPa), t is the testing time (day), E_1 is the elastic modulus (GPa), E_2 is the spring constant in visco-elastic phase (GPa), η_1 is the viscosity coefficient in steady-state phase (GPa. Day), and η_2 is the viscosity coefficient in transient phase (GPa.Day). Regression analyses on the octahedral shear strain-time curves based on Equation (5) using the SPSS statistical software (Wendai, 2000) are performed to determine the Burgers parameters for each salt specimen. Table 2 summarizes the calibration results.

The Lode parameter (μ) (Hunsche & Albrecht, 1990; Mellegard *et al.*, 2007; Zhang, Bai, & Francois, 2001) is used here to address the σ_2 effect on salt creep in three dimensions. It is calculated by:

$$\mu = -(2\sigma_2 - \sigma_3 - \sigma_1)/(\sigma_1 - \sigma_3) \quad (6)$$

The Lode parameter is equal to -1 for the triaxial extension testing, and equal to 1 for the triaxial compression testing. Figure 4 shows the Burgers parameters as a function of the Lode parameter (μ). The parameters η_1, E_2 and h_2 tend to decrease with increasing the Lode parameter. The spring constant, E_1 corresponding to the instantaneous deformation of salt, tend to be independent of the Lode parameter.

The parameters η_1, E_2 and η_2 obtained from the triaxial extension ($\sigma_1=\sigma_2>\sigma_3$) are about 1-1.5 times greater than those obtained from the polyaxial loading conditions ($\sigma_1>\sigma_2>\sigma_3$). The triaxial compression condition yields in the lowest magnitudes of the three parameters. Linear equations are used

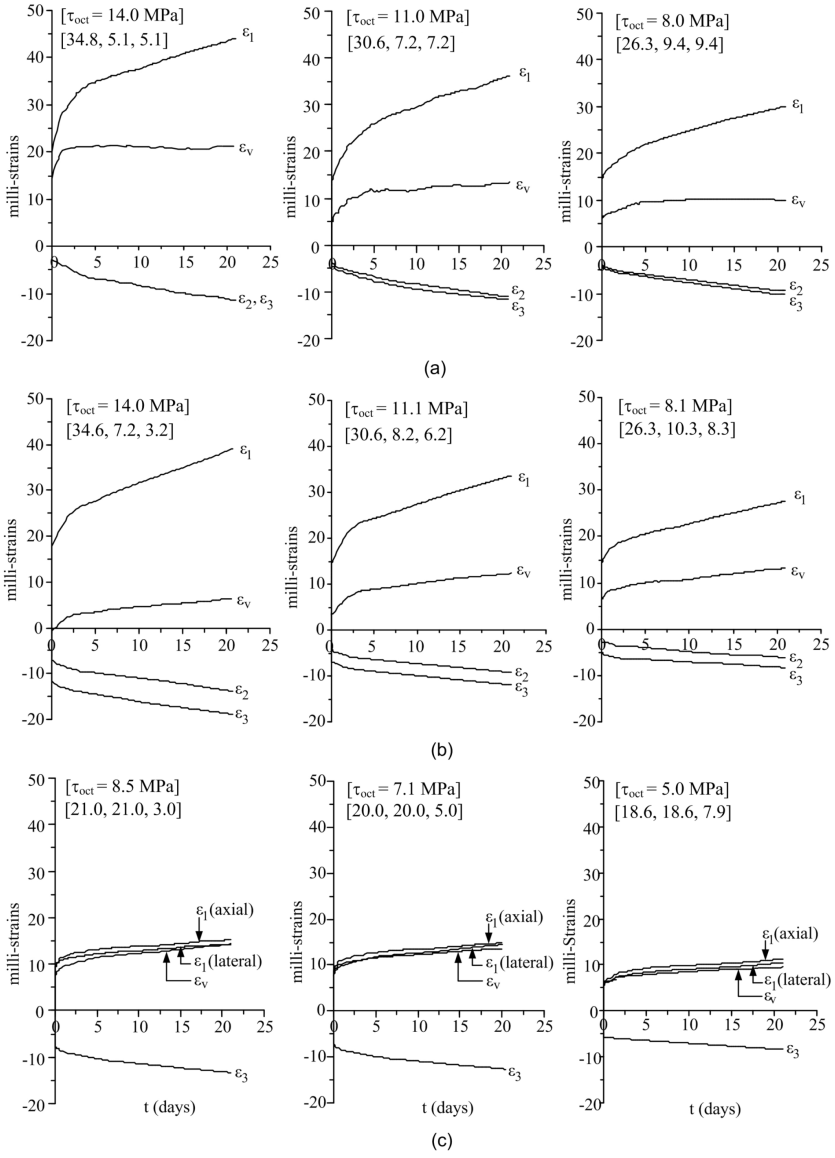

Figure 1. Strain-time curves obtained from triaxial compression (a), polyaxial compression (b) and triaxial extension (c). Numbers in bracket indicate [σ_1, σ_2, σ_3].

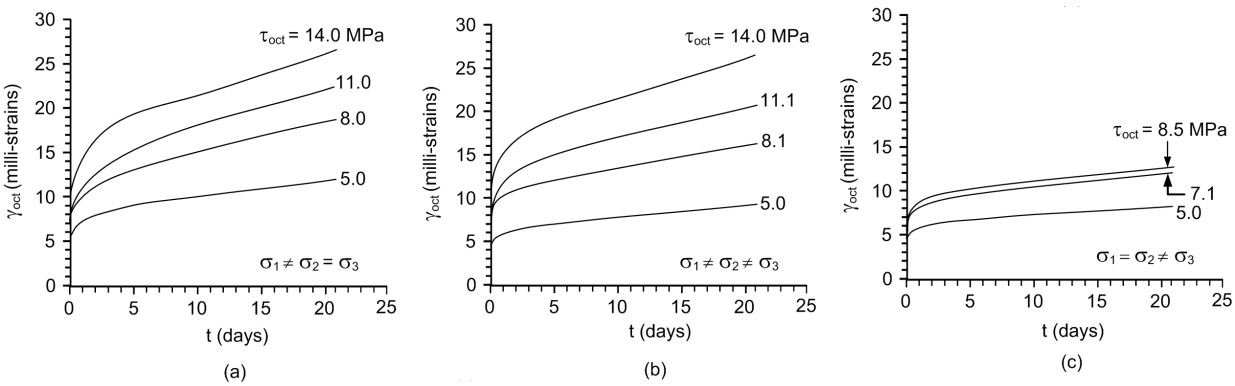

Figure 2. Octahedral shear strains (γ_{oct}) as a function of time obtained from triaxial compression (a), polyaxial compression (b) and triaxial extension (c).

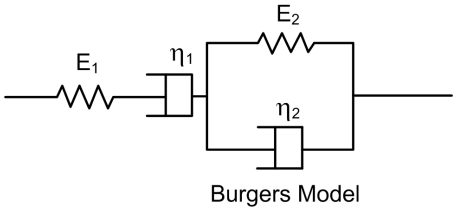

Figure 3. Modular components of the Burgers model.

to describe the variation of η_1, E_2 and η_2 with the Lode parameter, as follows:

$$\eta_1\{\mu\} = -\alpha_1 \times \mu + \alpha_2 \quad (7)$$

$$E_2\{\mu\} = -\beta_1 \times \mu + \beta_2 \quad (8)$$

$$\eta_2\{\mu\} = -\gamma_1 \times \mu + \gamma_2 \quad (9)$$

where α_1, β_1 and γ_1 are empirical constants equal to 8.935 GPa·day, 0.397 GPa and 0.516 GPa·day for the Maha Sarakham salt, and the constants α_2, β_2 and γ_2 equal to 38.48 GPa·day, 2.89 GPa and 3.98 GPa·day. By substituting Equations (7) through (9) into Equation (5) the octahedral shear strain can be defined as a function of Lode parameter in the form of the

Table 2. Burgers parameters calibrated from each salt specimen.

Loading conditions	μ	τ_{oct} (MPa)	Burgers Parameters			
			E_1 (GPa)	E_2 (GPa)	η_1 (GPa.day)	η_2 (GPa.day)
Triaxial Compression ($\sigma_1 \neq \sigma_2 = \sigma_3$)	1.00	14.0	1.15	2.80	32	4.0
	1.00	11.0	1.20	2.60	26	3.8
	1.00	8.0	1.03	2.10	23	3.5
	1.00	5.0	0.91	1.80	27	2.8
Polyaxial Compression ($\sigma_1 \neq \sigma_2 \neq \sigma_3$)	0.75	14.0	1.20	2.70	32	3.0
	0.84	11.1	1.12	2.80	32	3.5
	0.78	8.1	0.98	2.90	31	3.9
	0.18	5.0	1.00	2.90	42	4.0
Triaxial Extension ($\sigma_1 = \sigma_2 \neq \sigma_3$)	-1.00	8.5	1.20	3.55	53	4.0
	-1.00	7.1	1.05	2.30	48	4.5
	-1.00	5.0	1.15	2.90	44	5.0

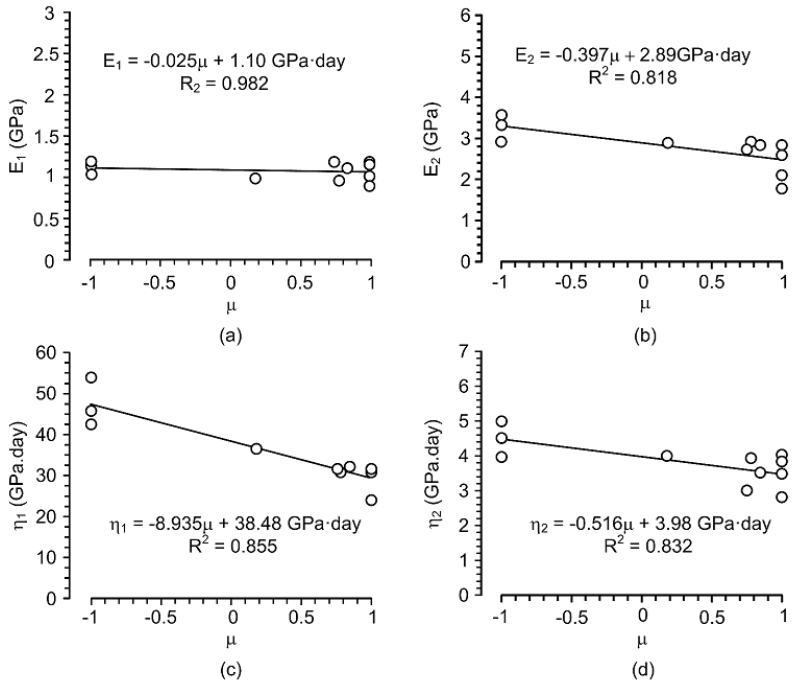

Figure 4. Burgers parameters as a function of Lode parameter (μ).

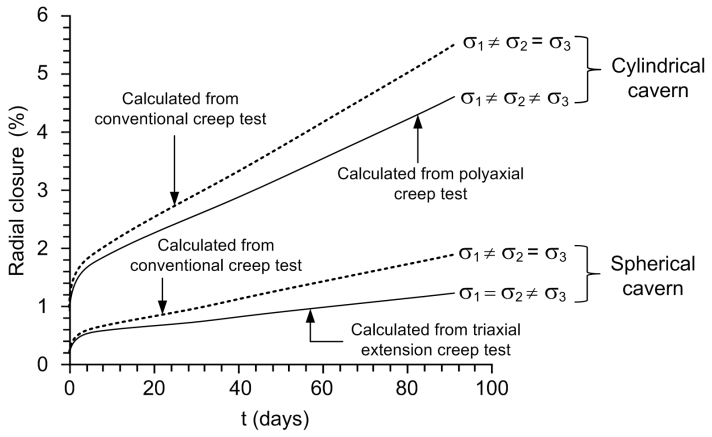

Figure 5. Closure of cavern wall as a function of time for cylindrical and spherical cavern shapes.

Burgers model. It can be used to calculate the time-dependent deformation of rock salt while considering the effect of σ_2.

6. Creep Closure of Storage Caverns

Sets of analytical solutions are derived to calculate radial displacements around cylindrical and spherical storage gas or compressed-air caverns in an infinite salt mass. These two cases are used here because their geometries impose the stress states that are different from that obtained from the conventional laboratory creep testing ($\sigma_1>\sigma_2=\sigma_3$). The salt is assumed to be time-independent under hydrostatic stress (i.e., linear visco-elastic material). It is recognized that the Burgers model is based on the linear visco-elastic theory. It may not truly represent the non-linear creep deformation of the in-situ salt around the cavern. The model is used here to demonstrate the effect of σ_2 obtained from the experimental result on the salt creep. The radial displacements (u_r) of cylindrical cavern are obtained from the Laplace transformation using time operator of the Burgers model which can be expressed as:

$$u_r = P_o[(A + B/9K) + (\alpha \cdot ((2A - B)/3))] - P_i r \alpha \quad (10)$$

$$A = [((1+k)/2) \times (r + (a^2/r))] + [((1-k)/2) \times (r - (a^4/r^3) + (4a^2/r))] \cos 2\theta \quad (11)$$

$$B = [((1+k)/2) \times (r - (a^2/r))] - [((1-k)/2) \times (r - (a^4/r^3))] \cos 2\theta \quad (12)$$

$$\alpha = (t/\eta_1) + (1/E_1) + (1/E_2) \times (1 - \exp(E_2 \times t/\eta_2)) \quad (13)$$

where P_i and P_o are an internal and external pressures, A and B are time-independent functions of position, K is bulk modulus, k is stress ratio, α is time-dependent function, θ is tangential coordinate, r is radius and a is inner boundary. Derivation of the α function is given in the Appendix section. For a spherical cavern under hydrostatic stresses the radial displacement (u_r) can be obtained from the following equations (Pariseau, 2012):

$$u_r = P_o[(1/18K) + (\alpha/3)] \cdot (a^3/r^2) + P_o[-(1/18K) + (\alpha/6)] \cdot (a^3/r^2) - [(P_i/2) \times (a^3/r^2) \cdot \alpha] \quad (14)$$

$$a = (t/\eta_1) + (1/E_1) + [(1/E_2) \cdot (1 - \exp(E_2 \times t/\eta_2))] \quad (15)$$

The creep parameters (Table 2) calibrated from the three loading conditions is used to determine the effect of intermediate principal stress on time-dependent closure of a salt cavern. In general, the salt around a cylindrical cavern is under polyaxial stresses state ($\sigma_\theta>\sigma_z>\sigma_r$). For the spherical cavern the surrounding salt is under triaxial extension stresses ($\sigma_\theta=\sigma_z>\sigma_r$). For this demonstration, the cylindrical cavern is taken as an upright cylinder with a diameter of 50 m. The spherical cavern also has a diameter of 50 m. The external pressure is calculated from the in-situ stress of 10.9 MPa which is equivalent to the depth of about 500 m. The storage cavern model is assumed to be subjected to the internal pressures of 2.2 MPa or about 20% of the in-situ stress at the cavern shoe, representing the minimum storage pressure of salt cavern. This is mainly to demonstrate the effect of σ_2 on the creep closure. The internal pressure is assumed to be uniform on the cavern boundaries.

Figure 5 compares the radial closure of the cylindrical and spherical caverns calculated by Equations (10) and (14) for 90 days. The radial closure obtained from the conventional compression creep test results is greater than that from the polyaxial compression and triaxial extension ($\sigma_1=\sigma_2>\sigma_3$) creep test results. The figure suggests that the conventional creep test results overestimate the actual closure of cylindrical and spherical caverns by as much as 15% and 35%, respectively. It should be noted that the calculation of cavern closure as demonstrated here is made under extreme loading condition, i.e., the internal pressure is left constant for long period (90 days). This is primarily to reveal the σ_2 effect on the creep closure of the storage caverns. In reality however

the storage caverns may not be allowed to subject to the low minimum storage pressure to longer than few days.

7. Discussions and Conclusions

The true triaxial creep test results indicate that the elastic deformation of salt, E_1, is not affected by the intermediate principal stress, σ_2. This agrees with the experimental results obtained by Sriapai and Fuenkajorn (2013) that the salt elastic deformation tends to be independent of σ_2. The intermediate principal stress affects both transient and steady-state creep phases of the Maha Sarakham salt. The creep strains decrease when σ_2 increases from σ_3 (triaxial compression) to σ_1 (triaxial extension). The visco-plastic coefficient η_1 and visco-elastic parameters (E_2 and η_2) tend to decrease with increasing the Lode parameter.

Under the simplified test conditions used here (i.e. constant mean stress and temperature) the Burgers model reveal the effect of σ_2 on the time-dependent deformation of the salt. The conventional creep test results may overestimate the actual closure of cylindrical and spherical caverns by about 15% and 35%, respectively. The findings imply that laboratory test results obtained from the conventional and commonly-used uniaxial and triaxial creep testing methods (e.g. ASTM D7070-08 standard practices) may over predict the time-dependent deformation of the actual in-situ salt under the true triaxial stress conditions.

It is recognized here that prediction of in-situ salt creep under true triaxial stresses using laboratory test data is difficult. Attempts have been made notably by Morgan and Wawersik (1989) who point out the discrepancies between the in-situ measurements at WIPP site and the creep model calibrated from the results of the thick-wall hollow cylinder under homogeneous and inhomogeneous loadings. The closure calculations presented in this paper is only to demonstrate the effect of σ_2 on the salt creep under simplified loading condition. The actual creep behavior of the salt around storage cavern would involve several factors that are not included in this study.

Acknowledgements

This study was funded by Suranaree University of Technology and by the Higher Education Promotion and National Research University of Thailand. Permission to publish this paper is gratefully acknowledged. We would like to thank Pimai Salt Co. for donating salt cores used in this study.

References

Al-Ajmi, A. M., & Zimmerman, R. W. (2005). Relation between the mogi and the coulomb failure criteria. *International Journal of Rock Mechanics and Mining Sciences*, *42*, 431-439. doi:10.1016/j.ijrmms.2004.11.004

American Society for Testing and Materials. (2008). *ASTM D7070-08, Standard test methods for creep of rock core under constant stress and temperature. West* Conshohocken, PA, Author.

Benz, T., & Schwab, R. (2008). A quantitative comparison of six rock failure criteria. *International Journal of Rock Mechanics and Mining Sciences*, *45*, 1176-1186. doi: 10.1016/j.ijrmms.2008.01.007

Cai, M. (2008). Influence of intermediate principal stress on rock fracturing and strength near excavation boundaries-Insight from numerical modeling. *International Journal of Rock Mechanics and Mining Sciences*, *45*, 763-72. doi:10.1016/j.ijrmms.2007.07.026

Colmenares, L. B., & Zoback, M. D. (2002). A statistical evaluation of intact rock failure criteria constrained by polyaxial test data for five different rocks. *International Journal of Rock Mechanics and Mining Sciences*, *39*, 695-729. doi: 10.1016/S1365-1609(02)00048-5

Fuenkajorn, K., Sriapai, T., & Samsri, P. (2012). Effects of loading rate on strength and deformability of Maha Sarakham salt. *Engineering Geology*, *135-136*, 10-23. doi:10.1016/j.enggeo.2012.02.012

Haimson, B. (2006). True triaxial stresses and the brittle fracture of rock. *Pure and Applied Geophysics*, *163*, 1101-1113. doi:10.1007/3-7643-7712-7_12

Haimson, B., & Chang, C. (2000). A new true triaxial cell for testing mechanical properties of rock, and its use to determine rock strength and deformability of Westerly granite. *International Journal of Rock Mechanics and Mining Sciences*, *37*, 285-96. doi:10.1016/S1365-1609(99)00106-9

Hunsche, U. (1984). Fracture experiments on cubic rock salt samples. In H. R. Hardy & M. Langer (Eds.), *Proceedings of the first conference on mechanical behavior of salt* (pp. 169-179). Clausthal-Zellerfeld, Germany: Trans Tech Publications.

Hunsche, U., & Albrecht, H. (1990). Results of true triaxial strength tests on rock salt. *Engineering Fracture Mechanics*, *35*(4/5), 867-877. doi:10.1016/0013-7944 (90)90171-C

Jaeger, J. C., Cook, N. G. W., & Zimmerman, R. W. (2007). *Fundamentals of rock mechanics*. London, England: Chapman and Hall.

Mellegard, K. D., DeVries, K. L., & Callahan, G. D. (2007). Lode angle effects on the creep of salt. *Proceedings of the 6th conference on the mechanical behavior of salt* (pp. 9-15). Hannover, Germany.

Morgan, H. S., & Wawersik, W. R. (1989). Computer and measured responses of a thick-walled hollow cylinder of salt subjected to both homogeneous and inhomogeneous loading. *Proceedings of the 30th U.S. symposium* (pp. 361-368). Brookfield, WI.

Obert, L., & Duvall, W. I. (1967). *Rock mechanics and the design of structures in rock*. New York, NY: Wiley.

Pariseau, G. W. (2012). *Design analysis in rock mechanic*. London, England: Taylor and Francis.

Phueakphum, D., Fuenkajorn, K., & Walsri, C. (2013). Effects of intermediate principal stress on tensile strength of rocks. *International Journal of Fracture*, *181*, 163-175. doi:10.1007/s10704-013-9829-0

Richards, J. (1993). *Plasticity and creep theory, examples, and problems*. Rochester, NY: Rochester Institute of Technology.

Sriapai, T., & Fuenkajorn, K. (2013). True-triaxial compressive strength of Maha Sarakham salt. *International Journal of Rock Mechanics and Mining Sciences*, *61*, 256-265. doi:10.1016/j.ijrmms.2013.03.010

Tiwari, R. P., & Rao, K. S. (2004). Physical modeling of a rock mass under a true triaxial stress state. *International Journal of Rock Mechanics and Mining Sciences*, *41*(Suppl.1), 396-401. doi:10.1016/j.ijrmms.2003.12.073

Tiwari, R. P., & Rao, K. S. (2006). Post failure behavior of a rock mass under the influence of triaxial and truetriaxial confinement. *Engineering Geology*, *84*, 112-29. doi: 10.1016/j.enggeo.2006.01.001

Warren, J. K. (1999). *Evaporites: their evolution and economics*. Oxford, England: Blackwell Science.

Wendai, L. (2000). Regression analysis, linear regression and probit regression, In 13 chapters. *SPSS for windows: Statistical analysis*. Beijing, China: House of Electronics Industry.

Yang, X. L., Zou J. F., & Sui Z. R. (2007). Effect of intermediate principal stress on rock cavity stability. *Journal of Central South University of Technology*, *14*(s1), 165-169. doi:10.1007/s11771-007-0237-3

You, M. (2009). True-triaxial strength criteria for rock. *International Journal of Rock Mechanics and Mining Sciences*, *46*, 115-127. doi:10.1016/j.ijrmms.2008.05.008

Zhang, K. S., Bai, J. B., & Francois, D. (2001). Numerical analysis of the influence of the Lode parameter on void growth. *International Journal of Solids and Structure*, *38*, 5847-5856. doi:10.1016/S0020-7683(00)00391-7

Zhou, S. A. (1994). Program to mode the initial shape and extent of borehole breakout. *Computers and Geosciences*, *20*(7-8), 1143-60. doi:10.1016/0098-3004(94)90068-X

Appendix A

Derivation of solutions for cylindrical and spherical cavern closure

The purpose of this appendix is to develop analytical solutions to calculate radial displacements around cylindrical and spherical cavities in an infinite plate of linear viscoelastic material subjected to a uniform stress field. The analysis is performed in plane strain. The material behavior is assumed to follow the Burgers model.

A-1 Cylindrical cavity in an infinite plate

The radial displacement around the cylindrical hole obtained from the elastic solution (Obert & Duvall, 1967) can be expressed as:

$$u_r = (1/E)[((\sigma_x+\sigma_y)/2)\cdot(r+(a^2/r))+((\sigma_x-\sigma_y)/2)\cdot(r-(a^4/r^3)+(4a^2/r))\cdot\cos2\theta] - (\nu/E)[(\sigma_x-\sigma_y)/2\cdot(r-(a^2/r))-((\sigma_x-\sigma_y)/2)\cdot(r-(a^4/r^3))\cdot\cos2\theta] \quad (A\text{-}1)$$

where σ_x, σ_y = lateral stresses, a = hole radius, E = Young's modulus, ν = Poisson's ratio, θ tangential coordinate. Let $\sigma_x = P$ and $\sigma_y = kP$, where P is a time-independent applied stress. Equation (A-1) becomes:

$$u = P/E\,(A) - P\nu/E\,(B) \quad (A\text{-}2)$$

where A and B are time-independent functions of position:

$$A = [((1+k)/2)\cdot(r+(a^2/r))]+[((1-k)/2)\cdot(r-(a^4/r^3)+(4a^2/r))]\cdot\cos2\theta \quad (A\text{-}3)$$

$$B = [((1+k)/2)\cdot(r-(a^2/r))]-[((1-k)/2)\cdot(r-(a^4/r^3))]\cdot\cos2\theta \quad (A\text{-}4)$$

where k = stress ratio (σ_y/σ_x). For the internal pressure term we can use a superposition law. Equation (A-2) becomes:

$$u = P/E\,(A) - P\nu/E\,(B) - P_i r/2G \quad (A\text{-}5)$$

where G is shear modulus

By taking Laplace transformations of Equation (A-2), they can be expressed in terms of transform variable "s" as follows:

$$\hat{u}(s) = [\hat{P}(s)/\hat{E}(s)]\,(A) - [\hat{P}(s)\times\hat{\nu}(s)/\hat{E}(s)]\,(B) - \hat{P}_i(s)\times\hat{r}(s)/2\hat{G}(s) \quad (A\text{-}6)$$

where $\hat{u}(s)$, $\hat{P}(s)$, $\hat{E}(s)$, $\hat{\nu}(s)$, $\hat{P}_i(s)$, $\hat{r}(s)$ and $\hat{G}(s)$ are the transformed operators.

Substituting $\hat{P}(s)$ by P/s, $\hat{r}(s)$ by r/s, $\hat{E}(s)$ by $(9K\hat{Q}_1/(\hat{Q}_1+6K\hat{P}_1)$, and $\hat{\nu}(s)$ by $(3K\hat{P}_1-\hat{Q}_1)/(\hat{Q}_1+6K\hat{P}_1)$ and Equation (A-6) becomes:

$$\hat{u}(s) = \{P_o/s\,(A)\,[(\hat{Q}_1+6K\hat{P}_1)/9K\hat{Q}_1]\} - \{P_o/s\,(B)\,[(3K\hat{P}_1-\hat{Q}_1)/9K\hat{Q}_1]\} - [(P_i r/s)(\hat{P}_1/\hat{Q}_1)] \quad (A\text{-}7)$$

where time operator of the Burgers model, $\hat{P}_1 = 1+(\eta_1/E_1+\eta 1/E_2+\eta_2/E_2)\cdot s+(\eta_1\eta_2/E_1E_2)\cdot s^2$ and $\hat{Q}_1 = \eta_2 s+(\eta_1\eta_2/E_2)\cdot s^2$ and performing inverse Laplace transformations, the radial displacements (u) around a circular hole in linear viscoelastic media can be expressed as:

$$u(t) = P_o\{[(1/9K)+(2/3)\alpha](A)-[-(1/9K)+(1/3)\alpha](B)-P_i r\alpha\} \quad (A\text{-}8)$$

By rearranging terms of Equation (A-8), they can be expressed in a simple form as:

$$u_r = P_o[(A+B/9K)+(\alpha\cdot((2A-B)/3))]-P_i r\alpha \quad (A\text{-}9)$$

$$\alpha = (t/\eta_1)+(1/E_1)+(1/E_2)\cdot(1-\exp(E_2\cdot t/\eta_2)) \quad (A\text{-}10)$$

A-2 Spherical cavity

For a spherical cavern under hydrostatic stress the radial displacement can be calculated as (Pariseau, 2012):

$$u_r = [(1+\nu)/2E]\,(a^3/r^2)\,(P) \quad (A\text{-}11)$$

To incorporate an internal pressure we can use superposition law, and hence Equation (A-11) becomes:

$$u_r = [(1+\nu)\,a^3/2Er^2]\,(P_o-P_i) \quad (A\text{-}12)$$

By taking Laplace transformations of Equation (A-2), it can be expressed in terms of transform variable "s" as follows:

$$\hat{u}(s) = [(\hat{P}_o(s)/2\hat{E}(s))+((\hat{P}_o(s)\cdot\hat{\nu}(s))/2\hat{E}(s))]\,(C) - [\hat{P}_i(s)/(4G)]\,(C) \quad (A\text{-}13)$$

where C is time-independent function of position ($C = a^3/r^2$). Using the time operator of the Burgers model and performing inverse Laplace transformation, the radial displacement (u_r) around a spherical cavity in linear viscoelastic media can be expressed as:

$$u_r = P_o[(1/18K)+(\alpha/3)]\cdot C + P_o[-(1/18K)+(\alpha/6)]\cdot C - (P_i/2\cdot C\cdot\alpha) \quad (A\text{-}14)$$